A Highly Conserved *Shh* Enhancer Coordinates Hypothalamic and Craniofacial Development

Zoe Crane-Smith[1], Jeffrey Schoenebeck[2], Katy A Graham[1], Paul S Devenney[1], Lorraine Rose[1], Mark Ditzell[3], Natasha Klenin[4], Deborah M Kurrasch[4], Laura A Lettice[1], and Robert E Hill[1,a]

[1] Medical Research Council Human Genetics Unit, Institute of Genetics and Molecular Medicine, University of Edinburgh, Edinburgh EH4 2XU, United Kingdom

[2] The Roslin Institute and Royal (Dick) School for Veterinary Studies, University of Edinburgh, Easter Bush, Midlothian, United Kingdom

[3] Cancer Research UK Edinburgh Centre, Institute of Genetics and Molecular Medicine, University of Edinburgh, Edinburgh EH4 2XU, United Kingdom

[4] Department of Medical Genetics, Alberta Children's Hospital Research Institute & Hotchkiss Brain Institute, University of Calgary, Calgary, AB T2N 4N1, Canada.

Running Title: Linking brain and cranial development

Key words: *Shh* / enhancer / hypothalamic development / craniofacial formation / embryonic development

[a] Corresponding author-

Robert Hill

Medical Research Council Human Genetics Unit,
Institute of Genetics and Molecular Medicine,
University of Edinburgh,
Edinburgh EH4 2XU,
United Kingdom

bob.hill@igmm.ed.ac.uk

ABSTRACT

Enhancers that are conserved deep in evolutionary time regulate characteristics held in common across taxonomic classes. Here, we deleted the highly conserved *Shh* enhancer SBE2 (*Shh* brain enhancer 2) which markedly reduced expression within the embryonic brain specifically in the rostral diencephalon; however, a putative secondary enhancer driving low levels of *Shh* partially compensated for the loss of SBE2. Further reduction of *Shh* levels, crossing the SBE2 deletion with the *Shh* null allele, disrupted brain and craniofacial tissue, linking SBE2 regulated expression to multiple defects and enabling analysis of development at different expression levels. Development of the hypothalamus, derived from the rostral diencephalon, was disrupted along both the anterior-posterior (AP) and the dorsal-ventral (DV) axes. DV patterning was highly sensitive to *Shh* expression levels, demonstrating a novel morphogenic context for*Shh*. In addition, loss of SBE2 activity in the diencephalon disrupted neighbouring craniofacial development, including the mediolateral patterning of the bones along the cranial floor and viscerocranium. Thus, SHH signalling coordinates hypothalamic morphogenesis with the formation of the adjacent midline cranial bones that consequently protects the neural tissue.

57

58 **Introduction**

59 Long-distance enhancers that are conserved across multiple classes of vertebrates
60 are implicated in regulating early embryonic development The *Shh* regulatory domain, which
61 extends for a 1Mb upstream of the gene contains a number of sequence elements identified
62 by high sequence conservation. These elements appear to be largely responsible for the
63 typical pattern of *Shh* expression observed at initial stages of organogenesis (Anderson et al.,
64 2014; Jeong et al., 2008). The deep conservation and early stages of expression mediated by
65 these *Shh* enhancers suggest that these regulators have a fundamental role in generating
66 ancient, shared vertebrate characteristics. Studies to date suggest a modularity in the
67 regulatory composition of *Shh* regulatory domain and thus, for at least some of the *cis*-
68 regulators, there is a simple relationship of a single enhancer to a distinct spatial domain of
69 expression (Jeong et al., 2006; Lettice et al., 2014); although, in other instances, secondary
70 enhancers provide compensatory low levels of expression (Letelier, et al., 2018; Tsukiji, et al.,
71 2014).

72 SHH is a signalling factor with a fundamental role in brain and craniofacial
73 development. A number of enhancers have been identified within the *Shh* regulatory domain
74 that are responsible for regulating expression in the midbrain and forebrain. Transgenic
75 analysis indicates that the SBE2 enhancer (Jeong et al., 2008, 2006; Zhao et al., 2012)
76 regulates *Shh* expression in the early developing forebrain, from the zona limitans
77 intrathalmica (ZLI) to the medial ganglionic eminence (MGE), specifically designated the
78 rostral diencephalon (Jeong et al., 2006; Zhao et al., 2012). Of particular interest is a clinically
79 relevant inactivating mutation in the SBE2 enhancer associated with features of semilobar
80 holoprosencephaly (Jeong et al., 2008). Holoprosencephaly (HPE) is a developmental
81 disorder of both the forebrain and midline facial structures which include microcephaly,
82 midfacial hypoplasia, cleft lip and palate, diabetes insipidus and moderate fusion of the
83 hypothalamus (Marcorelles and Laquerriere, 2010). More commonly, HPE is associated with
84 heterozygous mutations that inactivate the *Shh* gene (Ming and Muenke, 2002). These data

85 suggest that disruption of SBE2 driven expression in the early developing forebrain may
86 contribute to this disorder (Jeong et al., 2008).

87 Here, we deleted the SBE2 enhancer to discern the overall contribution to *Shh*
88 expression pattern and to establish links to the embryonic phenotype. *Shh* expression is
89 continuous throughout the central nervous system, relying on a number of *cis*-regulators to
90 generate the overall pattern (Anderson et al., 2014). The deletion of SBE2 interrupted this
91 spatial pattern by specifically downregulating expression in the ventral rostral diencephalon;
92 however, this reduction of SBE2 driven *Shh* expression produced no overt phenotype. We
93 identified a putative secondary enhancer responsible for residual levels of *Shh* expression that
94 compensated for the loss of SBE2 in the rostral diencephalon. Further reduction in expression
95 levels of *Shh* was attained by crossing the SBE2 deletion mice to the line carrying the *Shh* null
96 allele. The development of the hypothalamus and of the surrounding tissue was disrupted in
97 the compound mutants, linking diencephalic spatiotemporal expression to multiple defects and
98 enabling analysis of development at different expression levels. We show, firstly, that
99 patterning in the hypothalamus along the AP axis was disrupted but low levels of *Shh* are
100 sufficient for normal formation of the AP boundary. Further reductions in the levels of *Shh*,
101 however, led to misplaced spatial assignment due to disruption of the AP boundary. Secondly,
102 gene expression along the DV axis is, in contrast, concentration dependent and is consistent
103 with SHH functioning as a morphogen along this developmental axis, with tissue patterning
104 and eventual neuronal fate reliant upon varying concentrations of *Shh* signalling. Thirdly, we
105 find that loss of SBE2 activity disrupts craniofacial development affecting medial lateral
106 patterning of the bones along the cranial floor and palatal shelf, revealing that SBE2 directed
107 signalling from the brain directly regulates cranial and facial morphogenesis, providing further
108 evidence of the ventral patterning role played by *Shh* in craniofacial morphogenesis (Corman
109 et al., 2018; Dworkin et al., 2016). These data confirm that signalling in the brain has an
110 influence upon craniofacial morphology and raises an interesting evolutionary relationship that
111 links patterning of this crucial region of the brain with the formation of the bony plate barrier
112 underling this region in the skull. Hence, a single regulatory component coordinates the

113 combined function of directing brain development with the concomitant role of ensuring
114 physical neuroprotection.
115
116 **RESULTS**
117 **Loss of SBE2 enhancer activity leads to reduction in rostral diencephalic *Shh***
118 **expression**
119 To examine the role of the SBE2 enhancer during development, this element was
120 deleted using CRISPR/Cas9 (Cong et al., 2013) to remove 1.2 kb (Fig. S1A, B) containing the
121 conserved element. The SBE2 deleted allele, henceforth referred to as $Shh^{\Delta SBE2}$, was crossed
122 to generate homozygous embryos ($Shh^{\Delta SBE2/\Delta SBE2}$) and also to *Shh* null (Shh^{null}) mice to
123 generate compound heterozygous embryos ($Shh^{\Delta SBE2/null}$). Loss of the SBE2 enhancer alone
124 had no effect upon survival as the $Shh^{\Delta SBE2/\Delta SBE2}$ mice were viable and fertile and at weaning
125 no reduction in the number of mutant mice was found. Conversely, no live $Shh^{\Delta SBE2/null}$ offspring
126 were recorded by postnatal (P) 14 days (Fig. 1B), these compound heterozygous embryos
127 died perinatally failing to survive beyond P4. Normal ratios were observed at embryonic (E)
128 17.5 (Fig. 1A).
129 The rostral diencephalon, extending from the ZLI to the MGE, is the target for SBE2
130 expression as predicted by SBE2/reporter gene analysis in transgenic embryos (Jeong *et al*.,
131 2006). *Shh* mRNA expression analysis at E10.5 in $Shh^{\Delta SBE2/\Delta SBE2}$ and $Shh^{\Delta SBE2/null}$ embryos
132 revealed undetectable levels of *Shh* expression in the ventral portion of the rostral
133 diencephalon in both crosses (Fig. 1C-E), this region of the diencephalon will give rise to the
134 ventral portion of the tuberal and mammillary hypothalamus (Xie and Dorsky, 2017), and for
135 simplicity will henceforth be referred to as the ventral hypothalamus (VH). The region lacking
136 *Shh* expression in the SBE2 mutant embryos, however, was appreciably more restricted than
137 the region predicted by transgenic analysis, this is likely due to overlapping expression
138 caudally directed by other brain enhancers such as SBE3 and SBE4.
139 The differences in postnatal viability between $Shh^{\Delta SBE2/\Delta SBE2}$ and $Shh^{\Delta SBE2/null}$ suggested
140 that there may be residual, yet undetectable, *Shh* expression in the viable line. To investigate
141 possible low levels of *Shh* expression, patched-1 (*Ptch1*) expression, which is upregulated by

142 hedgehog signalling and is a sensitive readout of *Shh* expression, was examined (Casillas
143 and Roelink, 2018). Similar to the expression pattern observed for *Shh*, *Ptch1* was also
144 downregulated in the VH upon loss of SBE2 activity (Fig. 1F-H). However, in this instance,
145 levels differed between the compound heterozygous and the homozygous embryos. While
146 $Shh^{\Delta SBE2/null}$ embryos showed no detectable levels of *Ptch1* expression in the VH (Fig. 1H,
147 green arrow), the $Shh^{\Delta SBE2/\Delta SBE2}$ embryos presented residual levels (Fig. 1G, red arrow).
148 Therefore, low levels of *Shh* expression, which are undetectable by *in situ* hybridization, are
149 capable of rescuing the postnatal lethality.

150 To determine whether an additional regulator, perhaps a secondary enhancer, may
151 participate in directing rostral diencephalic expression, mice carrying an eGFP/Cre fusion
152 inserted into the *Shh* gene were used (Harfe et al., 2004). *Shh* expressing neural cells from
153 E10.5 disected brains were FAC sorted for analysis. ATAC-seq was used to identify stretches
154 of open chromatin as indicators of regulatory elements (Buenrostro et al., 2015). As expected,
155 a peak representing SBE2 was detected; however, in addition, a second peak (position
156 chr5:29230287-29230750 [mm9]), located ~436 kb away from the *Shh* promoter, was
157 observed (Fig. S2A). This peak contained a vertebrate conserved sequence element (Fig.
158 S2A) and when used in reporter constructs in transgenic embryos at E10.5 (Fig.S2B-D)
159 showed broad expression activity extending anteriorly from the midbrain into the diencephalon
160 (Fig. S2B-D). Other regions of expression that were appropriate to the *Shh* pattern, such as
161 in the midbrain and notochord, were also detected. Hence, this enhancer which we term FSE1
162 (forebrain secondary enhancer 1) is a good candidate for the regulator that rescues
163 development after SBE2 loss.

164

165 **Loss of SBE2 activity effects midline craniofacial deformities**

166 SBE2 deletion embryos were analysed for craniofacial malformations. Unsurprisingly,
167 given the postnatal viability of $Shh^{\Delta SBE2/\Delta SBE2}$ embryos, we did not observe any gross
168 craniofacial malformations nor deformities in the craniofacial skeletal elements (Fig S3A-B).
169 In contrast, at E17.5, $Shh^{\Delta SBE2/null}$ embryos appeared to present external head deformities, in

170 which the mutant embryos presented a more rounded head. To address whether these
171 changes in head shape were significant, control and *Shh*$^{\Delta SBE2/null}$ mutant embryos were subject
172 to geometric morphometric analysis to deconvolute the skull and test for differences between
173 control and mutant embryos. Centroid size, a proxy of skull scale, revealed that the compound
174 heterozygous mutant embryos tended to have an overall reduction in skull size, though this
175 did not reach significance (pairwise two-sample Wilcoxon, p=0.49) (Fig. 2A). Accordingly,
176 allometric shape variation due to size, genotype, and litter provided the best regression fit
177 (R^2=0.83, ANOVA p<0.001). Principal components of the non-allometric shape was also
178 explored. We observed clear, genotype-specific separation of control and mutant mice, with
179 the latter occupying a relatively broader expanse of morphospace (Fig. 2B). In mutants,
180 Principal Component 1 (46.5%) (Fig. 2B) describes a reduction in the anteroposterior axis
181 while dorsoventral and mediolateral axes expanded (Fig. 2C-H). Procrustes variances
182 between control and mutant mice were not significant, however this was presumably due to
183 limitations in statistical power. Indeed, shape differences described by PC1 were significant
184 (Welch Two Sample t-test, p=1.5x10^{-4}). OPT analysis revealed that, in addition to presenting
185 a perturbed overall head structure, *Shh*$^{\Delta SBE2/null}$ embryos displayed affected nasal cavities (Fig.
186 2J,L), which were reduced in length; however, the extent to which the nasal cavities were
187 affected varied between mutant embryos, with the example presented representing a
188 moderate phenotype. Moreover, a region of brain tissue, specifically the midline hypothalamic
189 tissue, was absent in the mutant embryos (Fig. 2I,K).

190 *Shh*$^{\Delta SBE2/null}$ embryos displayed midline craniofacial bone deformities with a high
191 degree of variability, which, based on phenotypic severity, were classified into three
192 categories: mild, moderate and severe (Fig. 3A-D). All mutant embryos presented defects in
193 the basisphenoid bone, ranging from the presence of a small remnant (Fig. 3B, pale green
194 arrow) to complete loss (Fig. 3C, D) and in the vomer bone, ranging from an excessive fusion
195 (Fig. 3B, yellow arrow) to complete absence (Fig. 3C, D). In addition, the moderate and severe
196 embryos displayed defects in the pterygoid and maxillary bones (Fig. 3C, D, white arrows).
197 Notably, all embryos showed some midline craniofacial element deformities, which indicates

198 that *Shh* signalling directed by SBE2 is involved in the midline development of the craniofacial
199 bones, and parallels the role *Shh* plays in early midline brain development (Choi et al., 2012).
200

201 **Mislocalized pituitary and loss of SHH signalling disrupts craniofacial development**

202 Closer examination of the heads of mutant compound heterozygous embryos revealed
203 that the basisphenoid bone, the most posterior defective cranial bone, was intercepted by the
204 adenohypophyseal pituitary lobe (Fig. 3E, F). This lobe of the pituitary was misplaced and
205 formed in a more anterior position, growing within the region where the basisphenoid will form
206 (the basis for the mislocalization is discussed below). Developmental timing of this event
207 suggests that the adenohypophysis disrupts this region before chondrogenesis initiates, which
208 indicates that the adenohypophyseal tissue likely presents a physical barrier to basisphenoid
209 development. The phenotypic variability may correlate with the extent to which the pituitary
210 lobe intercepted the basisphenoid bone in the mutant embryos.

211 Further investigations into the effect of SBE2 directed expression on craniofacial
212 development focused on mesenchymal *Ptch1* expression in the vicinity of the forebrain. In
213 control embryos at E12.5, *Ptch1* expression was detected within a narrow layer of
214 mesenchyme located directly adjacent to the floor of the diencephalon where *Shh* was
215 expressed (Fig. 4A-B). COL2A1, a type 2 collagen, is expressed during early cartilage
216 formation (Hissnauer et al., 2010) and co-localised with *Ptch1* in control embryos (Fig. 4E-F),
217 implicating that the underlying facial mesenchyme is under the influence of SHH and is
218 committed towards cartilage formation. At the same stage in the $Shh^{\Delta SBE2/null}$ embryos, *Ptch1*
219 expressing cells were absent in the underlying mesenchyme (Fig. 4C-D) and only a thin lining
220 of cells expressing COL2A1 was seen (Fig. 4G-H). The loss of *Ptch1* and COL2A1 staining
221 was found to be independent of the physical disruptive effects caused by mislocalisation of
222 the neurohypophysis, as the absence of both markers was evident in regions of the cranial
223 base which lie anterior to disrupted neurohypophyseal tissue detected in the mutant embryos
224 (Fig. 4C,G). Thus, SBE2 mediated *Shh* expression is instrumental in ensuring adequate cell
225 response and bone formation in the sub–diencephalic mesenchyme along the midline of the

226 palatal floor, and reduction of this cell population is critical for the midline craniofacial
227 phenotype.
228
229 **$Shh^{\Delta SBE2/null}$ embryos display mislocalised and deformed pituitary lobes due to**
230 **disruption of the AP hypothalamic boundary**
231 Pituitary lobe development was analysed at stages E11.5, E13.5 and E15.5. In
232 $Shh^{\Delta SBE2/null}$ mutant embryos at E11.5, Rathke's pouch (RP), which will give rise to the
233 adenohypophyseal lobe, and the infundibulum, which will give rise to the neurohypophyseal
234 pituitary lobe were both ectopically shifted ventrally (Fig. S4A, B). These findings reflect the
235 previous observations (Zhao et al., 2012) in conditional *Shh* deletion mice (recombination
236 driven by the SBE2 enhancer, designated SBE2-Cre), whereby an anterior shift in the pituitary
237 lobes was observed. At E13.5, RP and the infundibulum were still ectopically located in the
238 mutant embryos (Fig. 5A, C). Furthermore, RP was severely malformed in the mutant
239 embryos, while the infundibulum did not separate from the neuroectodermal tissue to the same
240 degree as control counterparts (Fig. 5A, C).
241 At E15.5, the adenohypohyseal lobe was more severely malformed in the mutant
242 embryos and remained ectopically located (Fig. S4C, D). Interestingly, at E17.5 the
243 neurophypophysis appeared absent in the mutant embryos (Fig. 3E, F), yet staining for
244 markers of neurohypophyseal tissue revealed that this was due to the lack of separation of
245 the neurohypophysis from the neuroectodermal tissue of origin (Fig. 5L, N). Moreover,
246 caspase-3 (CASP3) staining revealed that this remnant neurohypophyseal tissue appeared to
247 be undergoing apoptosis (Fig. 5M, O) indicating that inadequate neurohypophyseal
248 partitioning led to tissue degeneration. Despite the fact that both hypophyseal lobes were
249 misspecified in the $Shh^{\Delta SBE2/null}$ embryos early hypophyseal patterning was unperturbed (Fig.
250 S5C, F, I, L). These findings agree with observations by Zhao et al., (2012) in SBE2-Cre *Shh*
251 deletion mice, where pituitary markers, such as LHX3, were unperturbed despite hypophyseal
252 misplacement. However, whilst the SBE2 conditional *Shh* deletion mice displayed multiple
253 invagination sites for RP, only one site was observed in $Shh^{\Delta SBE2/null}$ embryos. While patterning

254 and early neuronal marker expression within the pituitary lobes appeared normal, at later
255 developmental stages, E17.5, neuronal populations within varied nuclei of the VH, which
256 establish connections with the pituitary lobes, were disrupted. Both the tyrosine hydroxylase
257 (TH1) (Fig. S6A-B) and the vasopressin neuronal population (Fig. S6E-F) of the
258 paraventricular nucleus (PVN) were lost in *Shh*$^{\Delta SBE2/null}$ embryos. Additionally, the oxytocin
259 neuronal population of the PVN was absent while the population found within the arcuate
260 nucleus (ARC) was either misspecified or mislocalised (Fig. S6C-D). These results indicate
261 that, in addition to the disruption of hypophyseal structure and location in development, the
262 appropriate neuronal connections, which are vital for the correct regulation of hormonal
263 release from the hypophyseal lobes, were also disrupted in the late embryonic mutants.

264 In *Shh*$^{\Delta SBE2/\Delta SBE2}$ mutant embryos, neither the adenohypophysis nor the
265 neurohypophysis was ectopically located and both lobes had separated from the tissue of
266 origin E13.5 (Fig. S3). Additionally, no defects were observed in early marker expression (Fig.
267 S5B, E, H, K); however, mild deformities were detected predominantly in the structure of the
268 lateral portion of adenohypophyseal lobe in *Shh*$^{\Delta SBE2/\Delta SBE2}$ mutant embryos (Fig. S3C-K).

269 Distinct anterior-posterior expression domains are established along the midline of the
270 hypothalamus by E9.5. The posterior hypothalamic domain expresses factors including *Bmp4*
271 and *Fgf10* whilst the anterior domain expresses *Six6*, *Tcf4* and *Shh*. Mutual inhibition between
272 these two gene expression domains exists, whereby in the absence of one domain the
273 opposing domain will expand to occupy the hypothalamic space (Ericson *et al*., 1998; Takuma
274 *et al*., 1998). The infundibulum expresses the posterior markers *Bmp4* and *Fgf10* and is
275 specified dorsally to the anterior hypothalamic tissue, at the AP transition zone (Ferrand,
276 1972; Kawamura and Kikuyama, 1995; Takuma *et al*., 1998; Treier *et al*., 1998). Inductive
277 cues from the hypothalamic tissue play a role in orchestrating the formation of RP (Schwind,
278 1928; Takuma *et al*., 1998). As RP and the infundibulum were both shifted ventrally in the
279 *Shh*$^{\Delta SBE2/null}$ mutant embryos (Fig. 5C), verification of any other associated defects in the
280 establishment of the AP hypothalamic boundary were sought. The posterior boundary of
281 expression of TCF4 was shifted ventrally in the mutant embryos (Fig. 5I) whereas the anterior

282 boundary of expression of *Fgf10* was shifted ventrally, expanding expression (Fig. 5F). The
283 shift observed for both the anterior and posterior markers was found to be significant in the
284 *Shh*$^{\Delta SBE2/null}$ mutant embryos (Fig. 5J, K). These results indicated that there is a shift in the AP
285 domain boundary with a reduction in anterior markers and gain of posterior markers. In the
286 *Shh*$^{\Delta SBE2/\Delta SBE2}$ mutant embryos no shift in expression of TCF4 (Fig. 5H) or *Fgf10* (Fig. 5E) was
287 observed, correlating with correct positioning of the pituitary lobes (Fig. 5C). These results
288 suggest that shift of the pituitary lobes occurs as a result of the aberrant specification of the
289 AP boundary, which does not appear to be sensitive to reduced levels of SHH, as shown in
290 *Shh*$^{\Delta SBE2/\Delta SBE2}$ embryos (Fig. S3C-F).

291

292 **Loss of SBE2 enhancer activity leads to defects in hypothalamic patterning in a**
293 **concentration dependent manner**

294 The hypothalamus, including the VH, can also be subdivided along the DV axis into
295 the floor, basal and alar plate, and within each subdivision different combinatorial gene
296 expression patterns can be identified (Puelles et al., 2012). DV hypothalamic patterning has
297 been greatly informed by the understanding of the patterning of the neural tube where distinct
298 neuronal progenitors are specified in response to the dorsal neural tube signals *Wnts* and
299 BMPs and the ventral neural tube signal *Shh* (Burbridge et al., 2016). In the developing
300 hypothalamus *Shh* is initially expressed from the prechordal mesoderm, it is subsequently
301 expressed along the floor plate and plays a role in inducing ventral hypothalamic fate
302 (Burbridge et al., 2016; Corman et al., 2018). In contrast, BMPs are expressed from the roof
303 of the telencephalon, regulating alar hypothalamic development (Burbridge et al., 2016). Given
304 that *Shh* signalling from the hypothalamic floor plate was reduced in the *Shh*$^{\Delta SBE2/\Delta SBE2}$ and
305 *Shh*$^{\Delta SBE2/null}$ mutant embryos, DV hypothalamic patterning was examined. Genes whose
306 expression are responsive to SHH levels in the neural tube were of particular interest. No
307 differences were detected between wild-type, *Shh*$^{\Delta SBE2/+}$ and *Shh*$^{null/+}$ embryos (Figure S7),

308 indicating that a 50% reduction in *Shh* levels has no effect upon DV patterning marker
309 expression.

310 Expression of the alar hypothalamic marker PAX6 and the opposing basal
311 hypothalamic marker NKX2-2 (Croizier et al., 2015; Guillemot, 2007) were examined. At E13.5
312 NKX2-2 was expressed along two stripes in the parasagittal regions of the hypothalamus, with
313 one stripe across the basal hypothalamus and another across the transition zone from the
314 basal-alar hypothalamus (Fig. 6A). In $Shh^{\Delta SBE2/\Delta SBE2}$ mutant embryos the dorsal stripe in the
315 basal hypothalamus was lost giving rise to a patchy appearance (Fig. 6B); while the
316 $Shh^{\Delta SBE2/null}$ mutant embryos were more severely affected, with both the alar-basal and basal
317 stripes absent (Fig. 6C). NKX2-2 expression is responsive to the low levels of *Shh* expression
318 observed in $Shh^{\Delta SBE2/\Delta SBE2}$, however these low levels are not sufficient to maintain the entirety
319 of the NKX2-2 population. The dorsal marker PAX6, which in control embryos was found only
320 within the alar hypothalamus (Fig. 6D), showed an expansion of expression dorsally into the
321 basal hypothalamic region in the $Shh^{\Delta SBE2/\Delta SBE2}$ mutant embryos (Fig. 6E). In $Shh^{\Delta SBE2/null}$
322 embryos, this dorsal expansion of PAX6 expression was more severe, with large patches of
323 PAX6 expression detected in the basal hypothalamus of the mutant embryos (Fig. 6F). These
324 results indicate that *Shh* signalling from the basal hypothalamus is required to restrict PAX6
325 expression solely to the alar region and that low levels of *Shh* activity, those found in basal
326 hypothalamus of $Shh^{\Delta SBE2/\Delta SBE2}$ mutants, are not sufficient to exclude PAX6 activity from this
327 region.

328 The expression of the transcription factors NKX6-1 and OLIG2, was also examined. In
329 control embryos OLIG2 was detected in the alar hypothalamus in a narrow region along the
330 edge of the third ventricle in sagittal and parasagittal regions (Fig. 6G); however, in
331 $Shh^{\Delta SBE2/\Delta SBE2}$ mutant embryos the OLIG2 positive cells showed a subtle dorsal shift away
332 from the edge of the third ventricle and additional expressing cells were detected in basal
333 hypothalamus (Fig. 6H). In $Shh^{\Delta SBE2/null}$ mutant embryos, OLIG2 positive staining cells had
334 dramatically shifted into the basal portion of the hypothalamus, with large areas of positive
335 staining cells detected (Fig. 6I). *Shh* activity acts to restrict OLIG2 expression to the alar

336 hypothalamus, whereupon reduction of SHH facilitates the spread of OLIG2 positive cells into
337 the basal hypothalamus.

338 In control embryos, NKX6-1 positive cells were also detected in the alar hypothalamus
339 in a narrow region along the edge of the third ventricle in sagittal and parasagittal regions (Fig.
340 6J); but in contrast to OLIG2, these cells were only detected along the basal lateral edge of
341 the third ventricle. In *Shh*$^{\Delta SBE2/\Delta SBE2}$ mutant embryos, NKX6-1 expression along the basal
342 lateral edge of the third ventricle was undetectable (Fig. 6K), but isolated groups of cells were
343 detected in the basal hypothalamus (Fig. 6K). *Shh*$^{\Delta SBE2/null}$ mutants showed complete loss of
344 the region of staining along the basal lateral edge with no additional regions of expression
345 observed (Fig. 6L). NKX6-1 appears to require low levels of *Shh* expression to be induced,
346 levels which are normally found along the edge of the third ventricle. In *Shh*$^{\Delta SBE2/\Delta SBE2}$ mutants
347 the levels of *Shh* expression are reduced within the basal hypothalamus to a level that allows
348 for ectopic expression of NKX6-1 within this region. In *Shh*$^{\Delta SBE2/null}$ mutants the complete loss
349 of the cells from the edge of the third ventricle indicate that the levels of *Shh* signalling activity
350 within the VH are insufficient to induce expression of NKX6-1.

351 The extent of changes in DV hypothalamic patterning correlate to the alteration in
352 levels of *Shh* expression, suggesting that *Shh* signalling is functioning in a concentration
353 dependent manner to induce ventral patterning in the hypothalamus. These results mirror the
354 role described for *Shh* in the neural tube, and involve many of the same key players, indicating
355 that *Shh* is acting as a morphogen within the VH to regulate tissue patterning.

356

357 **SBE2 enhancer activity controls downstream effects upon hypothalamic neuronal**
358 **populations**

359 We next sought to assess the downstream effects of disrupted DV patterning on
360 neuronal populations. As for the patterning markers, we first verified that there were no
361 detectable differences in the neuronal markers in the wildtype and heterozygotes, *Shh*$^{\Delta SBE2/+}$
362 and *Shh*$^{null/+}$ embryos (Figure S8), demonstrating that a 50% reduction in *Shh* levels has no
363 effect upon DV neuronal population specification. To examine the effect of disrupted DV

364 patterning upon the establishment of the different ventral hypothalamic neuronal populations,
365 we first analysed expression of the ventral hypothalamic neuronal marker NKX2-1 (Ohyama
366 et al., 2005). In control embryos at E13.5 NKX2-1 positive cells were detected across the
367 entirety of the basal hypothalamic domain (Fig. 7A). In *Shh*$^{\Delta SBE2/\Delta SBE2}$ mutant embryos the
368 region of NKX2-1 expressing cells was reduced and embedded within smaller domains
369 intermingled with patches devoid of staining (Fig. 7B). In the *Shh*$^{\Delta SBE2/null}$ mutant the region of
370 expression was further reduced with larger and more numerous patches devoid of positive
371 cells seen (Fig. 7C). ISL1 is a melanocortinogenic neuronal marker, in which positive cells are
372 detected throughout the hypothalamus (Kim et al., 2015). In control embryos positive staining
373 was detected throughout the basal hypothalamic region, as expected (Fig. 7D). No differences
374 in staining were detected between control and *Shh*$^{\Delta SBE2/\Delta SBE2}$ mutant embryos (Fig. 7E),
375 however, in *Shh*$^{\Delta SBE2/null}$ mutants there was substantial loss of positive staining cells in the
376 basal hypothalamus (Fig. 7F).

377 We additionally verified whether neurons that are restricted to specific nuclei of the
378 basal hypothalamus were affected upon removal of SBE2 activity. Steroidogenic factor 1
379 (SF1) positive neurons are known to be located in the ventromedial hypothalamus (VMH) and
380 are involved in the regulation of glucose metabolism and energy balance (Choi et al., 2013).
381 In control embryos SF1 positive neurons were detected in the basal hypothalamus, specifically
382 within the developing VMH (Fig. 7G). In *Shh*$^{\Delta SBE2/\Delta SBE2}$ mutant embryos the region of the basal
383 hypothalamus staining positively for SF1 was reduced (Fig. 7H), while in *Shh*$^{\Delta SBE2/null}$ mutant
384 embryos there was a complete loss of SF1 positive neurons (Fig. 7I). Somatostatin (SOM)
385 expressing neurons are a particular subset of GABAergic inhibitory neurons that are detected
386 in varied nuclei of the hypothalamus, including the VMH and the arcuate nucleus, which serve
387 to regulate cell proliferation ultimately affecting growth (Urban-Ciecko and Barth, 2016). In
388 control embryos, SOM neurons were detected in the basal hypothalamic region corresponding
389 to the arcuate nucleus at E13.5 (Fig. 7J). No differences were detected in *Shh*$^{\Delta SBE2/\Delta SBE2}$
390 mutant embryos where comparable staining was detected (Fig. 7K); however, in *Shh*$^{\Delta SBE2/null}$
391 mutant embryos no positive staining for SOM was detected in the VH (Fig. 7L). These results

392 indicated that, while the early low levels of *Shh* in the VH were sufficient to retain subsequent
393 specification of SOM neurons, higher levels of *Shh* activity were required to sustain the SF1
394 neuronal population in the basal hypothalamus. In the *Shh*$^{\Delta SBE2/null}$ mutant embryos both of
395 these populations were absent which indicated that early *Shh* activity was essential for the
396 maintenance of both the SF1 and SOM neuronal populations of the basal hypothalamus.
397

398 **Discussion**

399 **Secondary enhancer activity rescues SBE2 inactivation**

400 Loss of the highly conserved SBE2 in *Shh*$^{\Delta SBE2/\Delta SBE2}$ homozygous mice,
401 surprisingly,did not cause lethality or overt phenotypic effects in the brain and craniofacial
402 regions, which led to the identification of secondary enhancer activity from an element we
403 termed FSE1. Transgenic analysis consistently revealed broad expression activity throughout
404 the forebrain suggesting compensatory activity. Other embryonic expression domains
405 appropriate to the *Shh* pattern were also detected in transgenic embryos including the
406 midbrain, notochord and pharyngeal epithelium, all of which display *Shh* expression but are
407 driven by other known enhancer activities. This secondary enhancer, therefore, may be
408 responsible for co-regulation of *Shh* expression in other regions of the developing embryo. It
409 would be of interest to verify the effects of simultaneous removal of FSE1 and SBE2 function
410 upon the ventral hypothalamic neuronal population. For example, to ascertain whether
411 additional removal of the FSE1 enhancer would lead to a complete loss of the OLIG2 neuronal
412 population in the VH. If this were indeed the case, this would demonstrate that, similar to the
413 neural tube, *Shh* is also essential for OLIG2 expression in the VH, rather than solely being
414 required to ensure adequate restriction of expression to the alar hypothalamus.
415

416 **SBE2 mediated expression links brain and craniofacial development**

417 Heterozygous inactivating mutations in the *SHH* gene in patients cause HPE (Ming
418 and Muenke, 2002).while in mice complete loss of *Shh* leads to a multitude of phenotypic
419 consequences including the absence of the brain and craniofacial structures (Chiang *et al*.,

420 1996). While these observations highlight the links between brain and craniofacial
421 development, the question as to whether *Shh* signalling from the neuroectoderm is directly
422 required for the development of the craniofacial elements has remained largely unanswered.
423 Physical interactions between the brain and face begin early at the initial stages of facial
424 formation (Marcucio, et al., 2011). There are two fundamentally different mechanisms by
425 which development of the face and brain may be interrelated; firstly, the developing brain
426 serves as a dynamic architectural foundation upon which the face responds and develops or
427 secondly, signalling directly from the brain to the cranium and face regulates morphogenesis.
428 In fish, *Shh* signalling from both the oral ectoderm and neural tissue is required for
429 adequate progression of craniofacial development (Wada *et al*., 2005). In mammalian
430 development, *Shh* signalling from the oral ectoderm, which underlies the cranial base and also
431 neighbours the facial skeletal elements, has been demonstrated to be key in adequate
432 craniofacial development. Depletion of signalling from the oral ectoderm leads to defects in
433 the maxillary and mandibular bones, the palatine bones and the basisphenoid bone among
434 others (Jeong *et al*., 2004). The present study addressed the role of SBE2 forebrain
435 expression activity on the development of adjacent tissue which would be predicted to form
436 the midline of the cranial floor. Loss of SBE2 in the presence of the *Shh* null allele did lead to
437 both lethality and craniofacial deformities. Indeed, defects were observed in multiple skeletal
438 elements of the cranial base including the vomer bone and the basisphenoid bone, which
439 resides below the pituitary glands and the hypothalamic tissue. This demonstrated that *Shh*
440 signalling from the rostral diencephalon, which is regulated principally by the SBE2 enhancer,
441 is directly required for adequate craniofacial development to ensue.
442
443 **SBE2 affects both AP and DV patterning in the hypothalamus**
444 In addition to the craniofacial defects observed in the SBE2 mutant mouse lines,
445 defects in hypothalamic patterning were also observed. This is perhaps unsurprising given
446 that the region of *Shh* expression directed by SBE2 is the rostral diencephalon, the tissue from

447 which the hypothalamus originates. However, the mode in which *Shh* regulates patterning
448 within the hypothalamus appears to differ depending on the axis considered.

449 In relation to the AP axis, *Shh* directs patterning in a concentration independent
450 manner, whereby low, residual levels of signalling activity are sufficient to sustain normal
451 patterning, as the AP axis was unperturbed in the $Shh^{\Delta SBE2/\Delta SBE2}$ mutant embryos. In contrast,
452 in the $Shh^{\Delta SBE2/null}$ mutant embryos there was a loss of the anterior hypothalamic identity, which
453 is promoted by *Shh*, in favour of the posterior hypothalamic identity. A shift in the anterior
454 marker TCF4 was observed in the $Shh^{\Delta SBE2/null}$ mutant embryos, which contrasts observations
455 by Zhao *et al*., 2012, where a shift in all other AP hypothalamic markers with the exception of
456 TCF4 was seen. This difference likely resides in the different mouse lines used, whereby the
457 use of SBE-Cre to conditionally knock-down *Shh* activity may lead, firstly, to a temporal delay
458 in the removal of Shh activity and, secondly, to a broader removal of *Shh* activity than that
459 solely directed by SBE2. Notably, *Shh* is also required for adequate development of neuronal
460 populations which connect to the hypophyseal lobes and in turn, regulate hormonal release.
461 These results demonstrate a dual role for *Shh* in ensuring hypophyseal function, directly in
462 hypophyseal development and secondarily in regulating innervation.

463 In contrast to AP patterning along the DV hypothalamic axis was affected by *Shh*
464 activity in a concentration dependent manner. This is apparent in the $Shh^{\Delta SBE2/\Delta SBE2}$ mutant
465 embryos where defects in DV patterning, and also subsequent neuronal induction, were
466 observed. These defects were far less severe than those observed in the $Shh^{\Delta SBE2/null}$ mutant
467 embryos, where the disruption to DV patterning resulted in a complete loss of hypothalamic
468 neuronal populations. The results presented regarding DV hypothalamic patterning compare
469 to those described by Corman *et al*. (2018) where the same key neural tube patterning genes
470 and subsequence neuronal regulators are involved. However, we have demonstrated a novel
471 concentration dependent patterning activity of *Shh* in the hypothalamus, which has previously
472 only been described in the neural tube. Moreover, the results demonstrate loss of neuronal
473 populations beyond those of the dorsomedial, ventromedial and arcuate nuclei, implicating
474 additional neurons of the paraventricular nucleus, which play a key role in hypophyseal

475 regulation. Corman *et al*. (2018) also propose that NKX2-2 is expressed in a domain between
476 dorsal PAX6 and ventral NKX2-1, however, our data suggest that NKX2-1 is expressed
477 broadly across the entire ventral hypothalamic region and NKX2-2 is expressed in a
478 subdomain of the ventral hypothalamus, in regions overlapping with NKX2-1. It is entirely
479 possible that the ventral hypothalamic markers induced by *Shh*, including NKX2-2 are
480 responsible for inducing expression of NKX2-1, whereby the other ventral hypothalamic
481 markers, that are not completely absent in the $Shh^{\Delta SBE2/null}$ mutant embryos, sustain the
482 remaining NKX2-1 expression seen.

483 Similar to the patterning process in the neural tube, the response of different DV
484 patterning transcription factors to *Shh* was concentration dependent. For example, the OLIG2
485 expressing region was displaced ventrally in the $Shh^{\Delta SBE2/\Delta SBE2}$ mutants, an effect that was
486 further exacerbated in the $Shh^{\Delta SBE2/null}$ mutant embryos. In contrast, the NKX6-1 expressing
487 region moved ventrally in the $Shh^{\Delta SBE2/\Delta SBE2}$ mutants, yet was lost altogether in the VH region
488 along the lateral edge of third ventricle of $Shh^{\Delta SBE2/null}$ mutant embryos. These results indicate
489 that NKX6-1 is more sensitive to loss of *Shh* signalling than OLIG2. Indeed in the neural tube
490 OLIG2 responds to a wider window of *Shh* signalling levels than NKX6-1. This same variable
491 sensitivity to *Shh* signalling was seen for the neuronal populations, whereby only some of the
492 neuronal population that were disrupted in the $Shh^{\Delta SBE2/null}$ mutant embryos were also affected
493 in the $Shh^{\Delta SBE2/\Delta SBE2}$ mutants; for example, NKX2-1 expression required higher levels of *Shh*
494 expression than those needed for ISL1. However, the fact that some NKX2-1 positive neurons
495 persisted in $Shh^{\Delta SBE2/null}$ mutants, while the ISL1 population was nearly completely absent
496 indicates that low *Shh* signalling is essential for ISL1 expression while another factor may
497 likely contribute to the induction of NKX2-1, thus sustaining some of this population in
498 $Shh^{\Delta SBE2/null}$ mutants.

499 In addition, the SF1 neuronal population displayed a different response to the loss of
500 SBE2 than that seen for ISL1 and NKX2-1. In $Shh^{\Delta SBE2/null}$ mutants this population was absent,
501 indicating that *Shh* is essential for expression of SF1. Effects were also observed in
502 $Shh^{\Delta SBE2/\Delta SBE2}$ mutants, where the SF1 population was reduced, indicating that it is sensitive

503 to alterations in the normal levels of *Shh* activity, mirroring that seen for NKX2-1. Thus, early
504 SBE2 directed *Shh* signalling directs subsequent DV patterning in a concentration dependent
505 manner acting as a morphogen within ventral hypothalamic development, in which
506 transcription factor expression patterns are controlled by Shh levels which in turn instruct
507 ventral hypothalamic neuronal populations.
508

509 **SBE2 coordinates craniofacial development and patterning of the hypothalamus**

510 SBE2 regulates the expression of *Shh* in a region of the diencephalon in which SHH
511 signalling coordinates development of both the diencephalon and the neighbouring tissue
512 responsible for the cranial and facial bones, skeletal elements which are in turn responsible
513 for protecting the neural structures from external exposure. Homologues of the craniofacial
514 bones disrupted in mouse are found in species of all vertebrate classes from fish to mammals
515 (Maddin et al., 2016). In addition, the hypothalamus is an ancient hormone secreting centre
516 of the brain (Xie and Dorsky, 2017). We suggest that deep in vertebrate evolution SBE2
517 activity arose as a means to govern VH development and as a consequence of hypothalamus
518 proximity to craniofacial mesenchyme enabled *Shh* signalling to control formation of the bone
519 to ensure its own protection. We have demonstrated that disruptions to coordinated
520 development of the VH and cranial vault in mice leads to phenotypic defects which reflect
521 those seen for HPE patients. These results reveal not only that the interactions between the
522 brain and the face display deeply conserved evolutionary roots, but also show the key
523 importance of mouse models for addressing human disease phenotypes.
524

525 **Materials and methods**

526 **Embryo production and transgenic targeting**

527 Embryos were harvested at various embryonic stages between E10.5-E17.5. For all
528 experiments described triplicate datasets were used, unless otherwise stated. Reduction in
529 *Shh* levels to 50%, in $Shh^{null/+}$ embryos, is known to cause no phenotypic effects (Chiang et
530 al., 1996). Nevertheless, to allow for the use of littermate controls, differences between wild-

531 type, *Shh*$^{\Delta SBE2/+}$ and *Shh*$^{null/+}$ embryos were assessed for each experiment described. As
532 expected, no differences were detected in between the three previously mentioned genotypes,
533 as such all three genotypes were used as control embryos.
534 The expression driven by FSE1 was analysed in G0 transgenic embryos using a lacZ construct
535 which carried FSE1, a β-globin minimal promoter and LacZ as has been previously described
536 (Mackenzie et al., 1997). The FSE1 fragment was generated using PCR with the primers
537 GATCAT**GTCGAC**GCTCCAGGTACTGCTGTTCAG and
538 GATCAT**GCTGAC**ATGTGGATGGCAAGCATTGGC- the SalI restriction site used in the
539 cloning is highlighted in bold.
540
541 **ATAC-seq and FAC sorting**
542 Entire heads of GFP positive eGFP/Cre-*Shh* (Harfe et al., 2004) embryos were dissected and
543 single cell suspensions were made by incubating the dissected tissue in 1:5 dilution of
544 trypsin:versene at 37°C for 15 minutes. GFP positive cells were then sorted using a
545 fluorescence activated cell sorter. ATAC-seq libraries were made from the positive cell
546 population pooled across littermates as previously described (Buenrostro et al., 2015).
547 Subsequently libraries were subject to size selection to exclude DNA fragments larger than 1
548 kb using SPRIselect magnetic beads (Beckman Coulter). Samples were then sequenced on
549 a Illumina HiSeq 4000 platform to obtain 50 bp paired-end reads. Resulting reads were then
550 trimmed using cutadapt paired-end trimming, and subsequently aligned to the mm9 mouse
551 genome using bowtie2 paired-end alignment. Following alignment, unmapped and reads
552 mapped to the mitochondrial genome were then removed and duplicate reads were filteres
553 out using Picard MarkDuplicates. Once filtered reads were then shifted by +4bp for those
554 mapping to the positive strand and -5bp for those mapping to the negative strand. Broad peaks
555 were then called, to identify open chromatin regions, using MACS2 callpeak, using –g mm, -f
556 BEDPE, -B –broads and cutoff 0.01 options.
557
558 **SBE2 deletion line production by CRISPR**

559 Dual CRISPR guide oligo pairs were designed flanking the SBE2 enhancer region described
560 by Zhao, *et al* 2012. Subsequently, the pairs were annealed and cloned into the pX330 vector.
561 Guide sequences used were as follows:
562 Upstream of SBE2, 5' [Phos]AAACACATTAAAGCCCTCCAGCG 3'
563 and 5' [Phos]CACCGACGCTGGAGGGCTTTAATGT 3';
564 Downstream of SBE2, 5' [Phos]AAACACGAGCAAGCCAACCGGAGG 3' and 5'
565 [Phos]CACCGCTCCGGTTGGCTTGCTCGT 3'. CRISPR guides were then injected into single
566 cell stage C57 CBA F1 intercross embryos which were then implanted into CD1
567 pseudopregnant mice. G0 pups were genotyped and PCR products sent for sequencing to
568 confirm the presence of the correct deletions. Pups presenting the correct deletions were then
569 used to establish the line by mating to the C57BL/6J mice.
570

571 **OPT analysis**

572 OPT imaging was performed (Sharpe, 2003). Briefly, PFA-fixed embryos were embedded in
573 1% low-melting-point agarose and then immersed in methanol for 24 h to remove all water.
574 The embryos were then cleared for 24 h in BABB (one part benzyl alcohol/two parts benzyl
575 benzoate). The samples were then scanned using a Bioptonics 3001 scanner
576 (www.biooptonics.com) with images taken every 0.9° (of a 360° rotation). Upon completion,
577 images were reconstructed using Bioptonics proprietary software with the outputs then being
578 viewed with Dataviewer (Bioptonics) and Bioptonics Viewer.
579

580 **Morphometric analysis**

581 MicroCTs of fifteen E17.5 embryos (7 controls, 8 mutants) collected from three litters were
582 scanned post mortem using a Bruker Skyscanner 1076. Individual skull scans were
583 downsampled 2:1 using Bruker NRecon. Reconstructed images were converted to DICOM
584 format using Bruker DicomCT. Twenty-eight landmarks were placed on each isosurface using
585 Stratovan CheckPoint (v19.03.04.1102 Win64). In two mutants, dysmorphology of the vomer

586 prevented placement of corresponding landmarks and as such, the landmarks were indicated
587 as “missing”. Raw coordinates data saved in Morphologika format were processed in R
588 (v3.5.3) using Geomorph (v3.1.2), Rvcg (v0.18), Morpho (v2.7), and Hotelling (v1.0-5)
589 packages. Missing landmarks were estimated using a multivariate regression method
590 implemented in Geomorph. Following, a Generalised Procrustes analysis (GPA) translated,
591 rotated and rescaled raw landmark coordinate data to minimise the sum of squared distances
592 between specimens. The amount of rescaling required in the GPA is captured by the centroid
593 size, a variable which is used subsequently as a proxy for specimen size. A single outlier
594 (control, Litter 3) was removed as its Procrustes distance was >1 standard deviation from the
595 mean. Following removal of the outlier, the GPA was rerun to produce Procrustes shape
596 variables. To test for shape variation due to allometry, shape variables were regressed against
597 log(centroid size) as well as additional terms corresponding to genotype and litter. The best fit
598 included log(centroid size) interactions with both litter and genotype (ie coordinates ~
599 log(centroid size)*litter + log(centroid size)*genotype).

600 In order to visualise shape differences, a randomly chosen ply surface file was warped using
601 thin plate splines using the mean coordinate values of all fourteen specimens. The resulting
602 mesh represented the dataset reference which was subsequently warped to using principal
603 component minimum and maximum shape variables.

604 **Tissue processing**

605 Embryos were dissected at the stages indicated and fixed overnight at 4°C in 4%
606 paraformaldehyde (PFA) in phosphate-buffered saline (PBS). Embryos were washed briefly
607 in PBS, and then subject to serial passage through a sucrose gradient: 30 min in 5% sucrose
608 in PBS, 30 min in 10% sucrose in PBS then placed in 20% sucrose in PBS overnight at 4°C.
609 Embryos were then embedded in OCT compound and stored at -80°C. Sections were cut on
610 a cryostat at varying thicknesses appropriate to the embryonic stage: For E11.5 8 µm, for
611 E13.5 10 µm and for E17.5 14 µm.

612

613 **H&E staining**

614 Cryosections were allowed to reach room temperature then slides were then hydrated by
615 passage through 100% EtOH 3x 5 min then serial passage through 90%, 70%, 50% and lastly
616 30% EtOH for a couple of min each. Slides were washed in H_2O and then stained in
617 haemotoxylin for 4 min. They were then rinsed in H_2O and subsequently differentiated in
618 acid/alcohol for a few seconds. Slides were again rinsed in H_2O then placed in saturated
619 lithium carbonate solution for a few seconds. They were then rinsed in H_2O and stained in
620 eosin for 2 min then again rinsed in H_2O. Slides were then rinsed in 100% EtOH, placed in
621 fresh EtOH for 1 minute then placed in fresh EtOH 3x for 2 min each. Slides were then
622 passaged 3x through xylene for 5 min each, subsequently mounted in DPX (Cell Path, SEA-
623 1304-00A) and allowed to dry overnight.

624

625 ***lacZ* expression analysis, Dawson staining and wholemount *in situ* hybridisation**

626 Embryos were analysed for *lacZ* expression at E10.5 through staining for β-gal activity as
627 previously described (Mackenzie et al., 1997). Skeletal preparations from E17.5 foetuses were
628 stained simultaneously with Alizarin Red and Alcian Blue (Nagy et al., 2009a, 2009b). Whole-
629 mount *in situ* hybridisation on half heads was performed as previously described (Hecksher-
630 Sørensen et al., 1998).

631

632 ***In situ* hybridisation on cryosections**

633 Briefly, *in situ* probes were placed at 37°C for 5 mins, added to hybridisation buffer (1x salt (2
634 M NaCl, 100 mM Tris, 65 mM NaH_2PO_4, 50 mM Na_2HPO_4 and 50 mM EDTA in ddH_2O, pH to
635 7.5), 50% deionised formamide, 10% dextran sulfate, 1 mg/mL yeast RNA, 1x Denhardt's (2%
636 BSA, 2% Ficcoll, and 2% PVP made up to 100mL with ddH_2O)) pre-warmed to 65°C and
637 subsequently denatured at 95°C for 2 mins. Probes were then added to slides previously
638 allowed to reach room temperature. and placed in a 65°C waterbath overnight in a humidified
639 chamber with 5x SSC/50% formamide. Slides were subject to 3x 30 min washes at 65°C in
640 washing solution (50% formamide, 25 mL 1x SSC and 0.1% Tween 20 made up to 500 mL

641 Milli-Q H_2O) pre-warmed to 65°C. Subsequently, slides were washed 2x 30 min in 1x MABT
642 (100 mM maleic acid, 167 mM NaCl in ddH_2O, pH to 7.5, then 0.1% Tween 20). Slides were
643 blocked in 1x MABT + 2% blocking reagent + 20% heat inactivated sheep serum. A 1/2500
644 dilution of anti-DIG (Roche, 1109327490) in 1x MABT + 20% heat inactivated sheep serum
645 was then added and slides were placed in a humified chamber and allowed to incubate
646 overnight at room temperature. Slides were washed 5x for 20 min in 1x MABT. They were
647 then washed with NTMT (100 mM NaCl, 50 mM MgCl, 100 mM Tris pH 9.5 and 0.1% Tween
648 20 made up in ddH_2O) for 10 min followed by NTMTL (NTMT + 5 mM Levamisole) for 10 min.
649 Staining solution, NTMTL containing 3.75 µL/mL BCIP (Roche, 11383221001) and 5 µL/mL
650 NBT (Roche, 11383213001), was then added and slides were placed at 37°C to allow stain to
651 develop. Slides were immersed in H_2O, allowed to dry then mounted using Prolong gold
652 (Thermo Fisher, P39634).
653
654 **Immunofluorescence**
655 Cryosections were removed from the -80°C freezer and allowed to reach room temperature
656 before being subjected to antigen retrieval using a citric acid solution (10 mM citric acid
657 dissolved in ddH_2O, then pH to 6-6.5). Subsequently, slides were washed twice for 5 min in
658 PBS then blocked using 10% goat serum in PBT (0.1% Triton-X100 in PBS), with the
659 exception of PITX2 where anti-donkey serum was used, for 1 h at room temperature. Slides
660 were incubated in primary antibodies diluted in blocking solution overnight at 4°C as follows:
661 rabbit anti-CASP3 (1:500, Abcam, ab49822); mouse anti-COL2A1 (1:400, Santa Cruz, sc-
662 52659); rabbit anti-ISL1 (1:200, Abcam, ab20670); rabbit anti-LHX3 (1:250, Abcam, ab14555);
663 rabbit anti-NKX2-1 (1:250, Abcam, ab76013); rabbit anti-NKX2-2 (1:250, Abcam, ab191077);
664 rabbit anti-NKX6-1 (1:250, Abcam, ab221549); rabbit anti-OLIG2 (1:200, Abcam, ab109186);
665 rabbit anti-oxytocin (1:500, Abcam, ab212193); rabbit anti-PAX6 (1:350, Abcam, ab195045);
666 sheep anti-PITX2 (1:200, R&D, AF7388); rabbit anti-SF1 (1:200, Abcam, ab65815); rabbit
667 anti-TBX3 (1:200, Abcam, ab99302); rabbit anti-TH1 (1:200, Abcam, ab137869); rabbit anti-
668 TCF4 (1:100, Cell Signalling; C48H11); rabbit anti-vasopressin (1:500, Abcam, ab213707).

669 Slides were then washed 3 times for 10 min each in PBT and incubated for 1 h at room
670 temperature with fluorescent secondary antibodies in PBT in the dark, secondaries as follows:
671 goat anti-rabbit 488 (1:500, Thermo Fisher, A11034); goat anti-mouse 488 (1:500, Thermo
672 Fisher, A11029); donkey anti-sheep (1:500, Thermo Fisher, A11016). Slides were then
673 washed 3 times for 10 min each in PBT and subsequently stained with 1:10,000 DAPI in PBS
674 for 10 min, then washed in PBS twice for 5 min each. Lastly, slides were mounted using
675 Prolong Gold (Thermo Fisher, P39634) and allowed to dry prior to imaging.
676

677 **References**

678 Anderson, E., Devenney, P.S., Hill, R.E., and Lettice, L.A. (2014). Mapping the Shh long-
679 range regulatory domain. Development *141*, 3934–3943.

680 Buenrostro, J.D., Wu, B., Chang, H.Y., and Greenleaf, W.J. (2015). ATAC-seq: A Method for
681 Assaying Chromatin Accessibility Genome-Wide. Curr. Protoc. Mol. Biol. *109*, 21.29.1-9.

682 Burbridge, S., Stewart, I., and Placzek, M. (2016). Development of the Neuroendocrine
683 Hypothalamus. In Comprehensive Physiology, (Hoboken, NJ, USA: John Wiley & Sons,
684 Inc.), pp. 623–643.

685 Casillas, C., and Roelink, H. (2018). Gain-of-function Shh mutants activate Smo cell-
686 autonomously independent of Ptch1/2 function. Mech. Dev. *153*, 30–41.

687 Chiang, C., Ying, L.T.T., Lee, E., Young, K.E., Corden, J.L., Westphal, H., and Beachy, P.A.
688 (1996). Cyclopia and defective axial patterning in mice lacking Sonic hedgehog gene
689 function. Nature *383*, 407–413.

690 Choi, K.-S., Lee, C., and Harfe, B.D. (2012). Sonic hedgehog in the notochord is sufficient
691 for patterning of the intervertebral discs. Mech. Dev. *129*, 255–262.

692 Choi, Y.-H., Fujikawa, T., Lee, J., Reuter, A., and Kim, K.W. (2013). Revisiting the Ventral
693 Medial Nucleus of the Hypothalamus: The Roles of SF-1 Neurons in Energy Homeostasis.
694 Front. Neurosci. *7*.

695 Cong, L., Ran, F.A., Cox, D., Lin, S., Barretto, R., Habib, N., Hsu, P.D., Wu, X., Jiang, W.,
696 Marraffini, L.A., et al. (2013). Multiplex genome engineering using CRISPR/Cas systems.
697 Science *339*, 819–823.

698 Corman, T.S., Bergendahl, S.E., and Epstein, D.J. (2018). Distinct temporal requirements for
699 Sonic hedgehog signaling in development of the tuberal hypothalamus. Development *145*,
700 dev167379.

701 Croizier, S., Chometton, S., Fellmann, D., and Risold, P.-Y. (2015). Characterization of a
702 mammalian prosencephalic functional plan. Front. Neuroanat. *8*, 161.

703 Dworkin, S., Boglev, Y., Owens, H., Goldie, S., Dworkin, S., Boglev, Y., Owens, H., and
704 Goldie, S.J. (2016). The Role of Sonic Hedgehog in Craniofacial Patterning, Morphogenesis
705 and Cranial Neural Crest Survival. J. Dev. Biol. *4*, 24.

706 Ericson, J., Norlin, S., Jessell, T.M., and Edlund, T. (1998). Integrated FGF and BMP
707 signaling controls the progression of progenitor cell differentiation and the emergence of
708 pattern in the embryonic anterior pituitary. Development *125*, 1005–1015.

709 Ferrand, R. (1972). [Experimental study of the factors in cytological differentiation of the
710 adenohypophysis in the chick embryo]. Arch. Biol. (Liege). *83*, 297–371.

711 Guillemot, F. (2007). Spatial and temporal specification of neural fates by transcription factor
712 codes. Development *134*, 3771–3780.

713 Harfe, B.D., Scherz, P.J., Nissim, S., Tian, H., McMahon, A.P., and Tabin, C.J. (2004).
714 Evidence for an Expansion-Based Temporal Shh Gradient in Specifying Vertebrate Digit
715 Identities. Cell *118*, 517–528.

716 Hecksher-Sørensen, J., Hill, R.E., and Lettice, L. (1998). Double Labeling for Whole-Mount

717 In Situ Hybridization in Mouse. Biotechniques *24*, 914–918.

718 Hissnauer, T.N., Baranowsky, A., Pestka, J.M., Streichert, T., Wiegandt, K., Goepfert, C.,
719 Beil, F.T., Albers, J., Schulze, J., Ueblacker, P., et al. (2010). Identification of molecular
720 markers for articular cartilage. Osteoarthr. Cartil. *18*, 1630–1638.

721 Jeong, Y., Leskow, F.C., El-Jaick, K., Roessler, E., Muenke, M., Yocum, A., Dubourg, C., Li,
722 X., Geng, X., Oliver, G., et al. (2008). Regulation of a remote Shh forebrain enhancer by the
723 Six3 homeoprotein. Nat. Genet. *40*, 1348–1353.

724 Jeong, Y.S., El-Jaick, K., Roessler, E., Muenke, M., and Epstein, D.J. (2006). A functional
725 screen for sonic hedgehog regulatory elements across a 1 Mb interval identifies long-range
726 ventral forebrain enhancers. Development *133*, 761–772.

727 Kawamura, K., and Kikuyama, S. (1995). Induction from posterior hypothalamus is essential
728 for the development of the pituitary proopiomelacortin (POMC) cells of the toad (Bufo
729 japonicus). Cell Tissue Res. *279*, 233–239.

730 Kim, N., Park, C., Jeong, Y., and Song, M.-R. (2015). Functional Diversification of Motor
731 Neuron-specific Isl1 Enhancers during Evolution. PLOS Genet. *11*, e1005560.

732 Lettice, L.A., Williamson, I., Devenney, P.S., Kilanowski, F., Dorin, J., and Hill, R.E. (2014).
733 Development of five digits is controlled by a bipartite long-range cis-regulator. Development
734 *141*, 1715–1725.

735 Mackenzie, M.A.F., Jordan, S.A., Budd, P.S., and Jackson, I.J. (1997). Activation of the
736 Receptor Tyrosine Kinase Kit Is Required for the Proliferation of Melanoblasts in the Mouse
737 Embryo. Dev. Biol. *192*, 99–107.

738 Maddin, H.C., Piekarski, N., Sefton, E.M., and Hanken, J. (2016). Homology of the cranial
739 vault in birds: new insights based on embryonic fate-mapping and character analysis. R.
740 Soc. Open Sci. *3*, 160356.

741 Marcorelles, P., and Laquerriere, A. (2010). Neuropathology of holoprosencephaly. Am. J.
742 Med. Genet. Part C Semin. Med. Genet. *154C*, 109–119.

743 Ming, J.E., and Muenke, M. (2002). Multiple Hits during Early Embryonic Development:
744 Digenic Diseases and Holoprosencephaly. Am. J. Hum. Genet. *71*, 1017–1032.

745 Nagy, A., Gertsenstein, M., Vintersten, K., and Behringer, R. (2009a). Alcian blue staining of
746 the mouse fetal cartilaginous skeleton. Cold Spring Harb. Protoc. *2009*, pdb.prot5169.

747 Nagy, A., Gertsenstein, M., Vintersten, K., and Behringer, R. (2009b). Alizarin Red Staining
748 of Post-natal Bone in Mouse. Cold Spring Harb. Protoc. *2009*, pdb.prot5171-pdb.prot5171.

749 Ohyama, K., Ellis, P., Kimura, S., and Placzek, M. (2005). Directed differentiation of neural
750 cells to hypothalamic dopaminergic neurons. Development *132*, 5185–5197.

751 Puelles, L., Martinez-de-la-Torre, M., Bardet, S., and Rubenstein, J.L.R. (2012).
752 Hypothalamus. Mouse Nerv. Syst. 221–312.

753 Schwind, J.L. (1928). The development of the hypophysis cerebri of the albino rat. Am. J.
754 Anat. *41*, 295–319.

755 Sharpe, J. (2003). Optical projection tomography as a new tool for studying embryo
756 anatomy. J. Anat. *202*, 175–181.

757 Takuma, N., Sheng, H.Z., Furuta, Y., Ward, J.M., Sharma, K., Hogan, B.L., Pfaff, S.L.,
758 Westphal, H., Kimura, S., and Mahon, K.A. (1998). Formation of Rathke's pouch requires
759 dual induction from the diencephalon. Development *125*, 4835–4840.

760 Treier, M., Gleiberman, A.S., O'Connell, S.M., Szeto, D.P., McMahon, J.A., McMahon, A.P.,
761 and Rosenfeld, M.G. (1998). Multistep signaling requirements for pituitary organogenesis in
762 vivo. Genes Dev. *12*, 1691–1704.

763 Urban-Ciecko, J., and Barth, A.L. (2016). Somatostatin-expressing neurons in cortical
764 networks. Nat. Rev. Neurosci. *17*, 401–409.

765 Xie, Y., and Dorsky, R.I. (2017). Development of the hypothalamus: conservation,
766 modification and innovation. Development *144*, 1588–1599.

767 Zhao, L., Zevallos, S.E., Rizzoti, K., Jeong, Y., Lovell-Badge, R., and Epstein, D.J. (2012).
768 Disruption of SoxB1-Dependent Sonic hedgehog Expression in the Hypothalamus Causes
769 Septo-optic Dysplasia. Dev. Cell *22*, 585–596.

770

771 **Figure legends**

772 **Figure 1. Loss of SBE2 leads to reduced *Shh* activity in the rostral diencephalon.** (A-B) Peri
773 and post-natal survival for $Shh^{\Delta SBE2/null}$ compound heterozygotes is shown. Statistical significance
774 was assessed using the Student's T-test (n=3). (C-E) *In situ* hybridisation for *Shh* in E10.5 day
775 heads bisected along the midline is shown for control, $Shh^{\Delta SBE2/\Delta SBE2}$ homozygotes and
776 $Shh^{\Delta SBE2/null}$ compound heterozygotes. The red and green arrows point to the rostral diencephalic
777 region where *Shh* expression is absent, while black arrows point to control expression. (F-H) *In*
778 *situ* hybridisation for *Ptch1* in E10.5 day bisected heads is shown. Wildtype levels of *Ptch1*
779 expression in rostral diencephalon in control embryos (indicated by black arrow in F), reduced
780 levels in $Shh^{\Delta SBE2/\Delta SBE2}$ (indicated by red arrows in G) and undetectable levels in $Shh^{\Delta SBE2/null}$
781 (indicated by green arrow in H) is shown.

782

783 **Figure 2. $Shh^{\Delta SBE2/null}$ embryos present an overall altered head shape and gross deformities.**
784 (A) Morphometric analysis of overall head size (log Csize- log centroid size) in control and
785 $Shh^{\Delta SBE2/null}$ heads at E17.5. (B) Morphometric analysis of overall head shape in control and
786 $Shh^{\Delta SBE2/null}$ heads at E17.5. (C-E) Ply surface of a control E17.5 day CT scanned skull, from a
787 dorsal, lateral and ventral angle. (F-H) Morphed ply of a randomly chosen control E17.5.surface,
788 morphed based on the average of $Shh^{\Delta SBE2/null}$ PC1 landmark changes, presented from a dorsal,
789 lateral and ventral angle. (control n=6; mutant n=8). (I-L) OPT scan stills from E17.5 day control
790 and $Shh^{\Delta SBE2/null}$ heads, presenting the midline sagittal plane and the coronal nasal region. Red
791 arrows point to the region of absent hypothalamic tissue seen in $Shh^{\Delta SBE2/null}$ embryos. Red lines
792 serve to demonstrate the reduced nasal cavities found in $Shh^{\Delta SBE2/null}$ embryos.

793

794 **Figure 3. $Shh^{\Delta SBE2/null}$ embryos present deformities in the bones of the cranial vault.** (A-D)
795 Dual staining highlighting chondrogenic (blue) and skeletal (red) craniofacial elements in control
796 and $Shh^{\Delta SBE2/null}$ E17.5 heads are shown. Pale green arrows indicate the basisphenoid bone,
797 yellow arrows indicate the vomer bone and the white arrows indicate the pterygoid bone. (E-F)
798 H&E staining of E17.5 day parasagittal cryosections from control and $Shh^{\Delta SBE2/null}$ heads. Black
799 arrows point to the region of the basisphenoid bone which is intercepted by the adenohypophysis

800 in *Shh*$^{\Delta SBE2/null}$ embryos. A zoomed out view of an E17.5 day head parasagittal cryosection is
801 depicted in (G). The yellow box presents the region of the head depicted in (E-F). AP-
802 adenohypophysis; NP- neurohypophysis; BS- basisphenoid bone; BP- base plate of the skull; NA-
803 nasal prominence; FB- forebrain; HB- hindbrain; TG- tongue.
804
805 **Fig. 4. Bone formation is abnormal in the viscerocranium of *Shh*$^{\Delta SBE2/null}$ embryos.** (A-D) *In*
806 *situ* hybridisation for *Ptch1* in E12.5 day coronal cryosections of control and *Shh*$^{\Delta SBE2/null}$ embryos.
807 (A&C) present the palatine region and (B&D) present the basisphenoid region. Black arrows point
808 to the region of *Ptch1* expression seen below the hypothalamic tissue which is absent in
809 *Shh*$^{\Delta SBE2/null}$ embryos. (I & K) Immunofluorescent staining for COL2A1 in E12.5 day coronal
810 cryosections of control and *Shh*$^{\Delta SBE2/null}$ embryos. (E&G) present the palatine region and (F&H)
811 present the basisphenoid region. Red arrows point to the region of COL2A1 expression seen below
812 the hypothalamic tissue which mostly is absent in *Shh*$^{\Delta SBE2/null}$ embryos. 3V- third ventricle; HP-
813 hypothalamus; TG- tongue; RP- Rathke's pouch. (n=3)
814
815 **Fig. 5. The AP hypothalamic boundary is shifted ventrally in *Shh*$^{\Delta SBE2/null}$ embryos.** (A-C)
816 H&E staining of E13.5 day sagittal cryosections of control, *Shh*$^{\Delta SBE2/\Delta SBE2}$ and *Shh*$^{\Delta SBE2/null}$
817 embryos. (D-F) *In situ* hybridisation for *Fgf10* in E11.5 day sagittal cryosections of control,
818 *Shh*$^{\Delta SBE2/\Delta SBE2}$ and *Shh*$^{\Delta SBE2/null}$ embryos. Red arrows represent the distance between the MGE
819 and the anterior boundary of *Fgf10* expression. (G-I) Immunofluorescent staining for TCF4 in
820 E11.5 day sagittal cryosections of control, *Shh*$^{\Delta SBE2/\Delta SBE2}$ and *Shh*$^{\Delta SBE2/null}$ embryos. White arrows
821 represent the distance between the posterior infundibulum and the posterior boundary of TCF4
822 expression. (J)- Quantification of the distance depicted by the red arrows in (D-F) in control,
823 *Shh*$^{\Delta SBE2/\Delta SBE2}$ and *Shh*$^{\Delta SBE2/null}$ embryos. (K)- Quantification of the distance between depicted by
824 the white arrows in (G-I) in control, *Shh*$^{\Delta SBE2/\Delta SBE2}$ and *Shh*$^{\Delta SBE2/null}$ embryos. (L & N)
825 Immunofluorescent staining for NKX2-1 in E17.5 day sagittal cryosections of control and
826 *Shh*$^{\Delta SBE2/null}$ embryos. (M & O) Immunofluorescent staining for CASP3 in E17.5 day sagittal
827 cryosections of control and *Shh*$^{\Delta SBE2/null}$ embryos. Red circles demarcate the region of cell death

828 apparent in mutant embryos. NS- not significant. BH- basal hypothalamus; IF- infundibulum; RP-
829 Rathke's pouch; MGE- medial ganglionic eminence.
830
831 **Fig. 6. DV hypothalamic patterning is affected by loss of SBE2.** (A-C) Immunofluorescent
832 staining for NKX2-2 in E13.5 day ventral hypothalamic (VH) parasagittal cryosections of control,
833 *Shh*$^{\Delta SBE2/\Delta SBE2}$ and *Shh*$^{\Delta SBE2/null}$ embryos. Red arrows point to the region of NKX2-2 expression in
834 the basal hypothalamus which is reduced or absent upon removal of SBE2 enhancer function. (D-
835 F) Immunofluorescent staining for PAX6 in E13.5 day VH parasagittal cryosections of control,
836 *Shh*$^{\Delta SBE2/\Delta SBE2}$ and *Shh*$^{\Delta SBE2/null}$ embryos. White arrows point to the region of ectopic PAX6
837 expression in the BH which is seen upon removal of SBE2 function. (G-I) Immunofluorescent
838 staining for OLIG2 in E13.5 day VH parasagittal cryosections of control, *Shh*$^{\Delta SBE2/\Delta SBE2}$ and
839 *Shh*$^{\Delta SBE2/null}$ embryos. White arrows point to the ectopic regions of expression of OLIG2 in the BH
840 which are seen upon removal of SBE2 function. (J-L) Immunofluorescent staining for NKX6-1 in
841 E13.5 day VH parasagittal cryosections of control, *Shh*$^{\Delta SBE2/\Delta SBE2}$ and *Shh*$^{\Delta SBE2/null}$ embryos. Red
842 arrows point to the region of NKX6-1 expression in the AH which is absent upon removal of SBE2
843 function whilst white arrows point to the region of ectopic expression in the BH seen in
844 *Shh*$^{\Delta SBE2/\Delta SBE2}$ embryos. AH- alar hypothalamus; BH- basal hypothalamus; IF- infundibulum; RP-
845 Rathke's pouch.
846
847 **Fig. 7. DV hypothalamic neuronal populations are affected by loss of SBE2.** (A-C)
848 Immunofluorescent staining for NKX2-1 in E13.5 day VH parasagittal cryosections of control,
849 *Shh*$^{\Delta SBE2/\Delta SBE2}$ and *Shh*$^{\Delta SBE2/null}$ embryos. Red arrows point to the regions devoid of NKX2-1
850 expression which are found upon removal of SBE2 function. (D-F) Immunofluorescent staining for
851 ISL1 in E13.5 day VH parasagittal cryosections of control, *Shh*$^{\Delta SBE2/\Delta SBE2}$ and *Shh*$^{\Delta SBE2/null}$
852 embryos. Red arrows point to the regions of the BH where ISL1 is mostly absent in *Shh*$^{\Delta SBE2/null}$
853 embryos. (G-I) Immunofluorescent staining for SF1 in E13.5 day VH parasagittal cryosections of
854 control, *Shh*$^{\Delta SBE2/\Delta SBE2}$ and *Shh*$^{\Delta SBE2/null}$ embryos. Red arrows point to the region of the BH where
855 SF1 expression is reduced or absent upon removal of SBE2 function. (J-L) Immunofluorescent
856 staining for somatostatin in E13.5 day VH parasagittal cryosections of control, *Shh*$^{\Delta SBE2/\Delta SBE2}$ and

857 *Shh*$^{\Delta SBE2/null}$ embryos. Red arrows point to the region of the BH where somatostatin is lost in
858 *Shh*$^{\Delta SBE2/null}$ embryos. A zoomed in view of the region of somatostatin expression is presented in
859 the green boxes in the upper right hand corner of (J & K). AH- alar hypothalamus; BH- basal
860 hypothalamus; IF- infundibulum; RP- Rathke's pouch.

A Embryonic day 17.5 (E17.5)

	Total no.	Control	Single het	Compound het
Observed	41	10	19	12
Expected	-	10	20	10

p=0.7985

B Post-natal day 14

	Total no.	Control	Single het	Compound het
Observed	24	4	20	0
Expected	-	6	12	6

p=0.0025

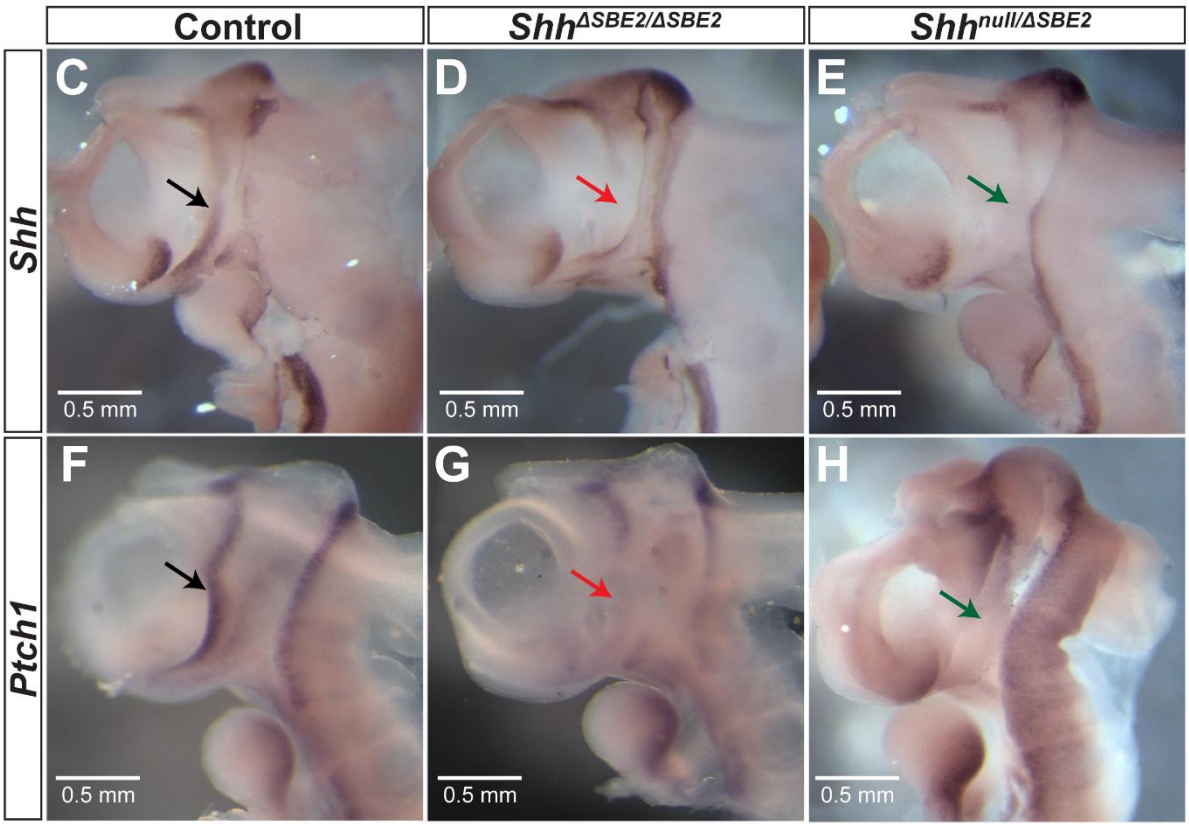

Figure 1

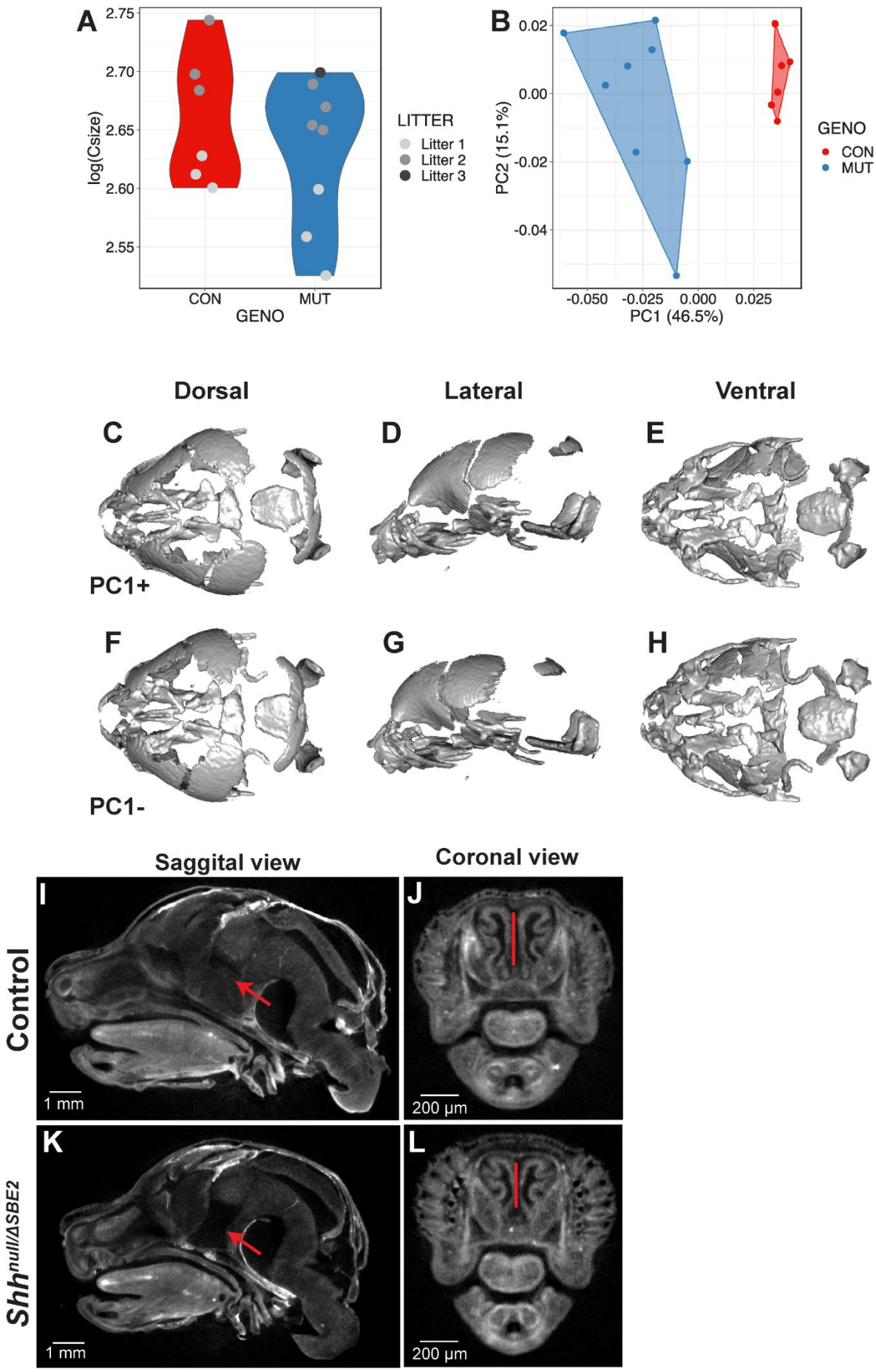
A
2.75
2.70
2.65
2.60
2.55
log(Csize)
CON
MUT
GENO
LITTER
Litter 1
Litter 2
Litter 3
B
0.02
0.00
-0.02
-0.04
PC2 (15.1%)
-0.050
-0.025
0.000
0.025
PC1 (46.5%)
GENO
CON
MUT
Dorsal
Lateral
Ventral
C
D
E
PC1+
F
G
H
PC1-
Saggital view
Coronal view
I
J
Control
1 mm
200 µm
K
L
Shh null/ΔSBE2
1 mm
200 µm

Figure 2

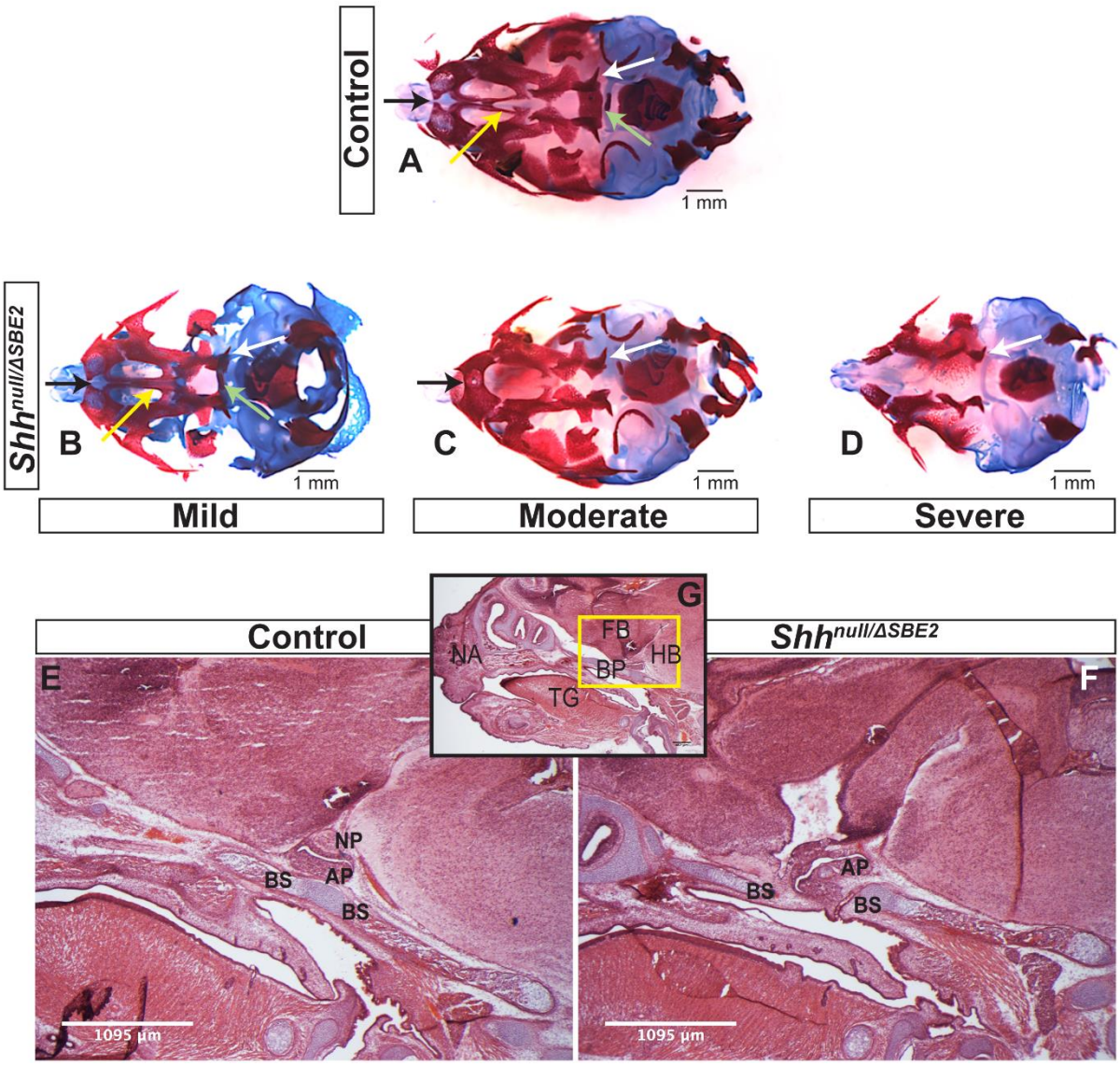
Control
A
1 mm
Shhnull/ΔSBE2
B
1 mm
C
1 mm
D
1 mm
Mild
Moderate
Severe
Control
Shhnull/ΔSBE2
E
F
G
NA
FB
HB
BP
TG
NP
AP
BS
BS
AP
BS
BS
1095 µm
1095 µm

Figure 3.

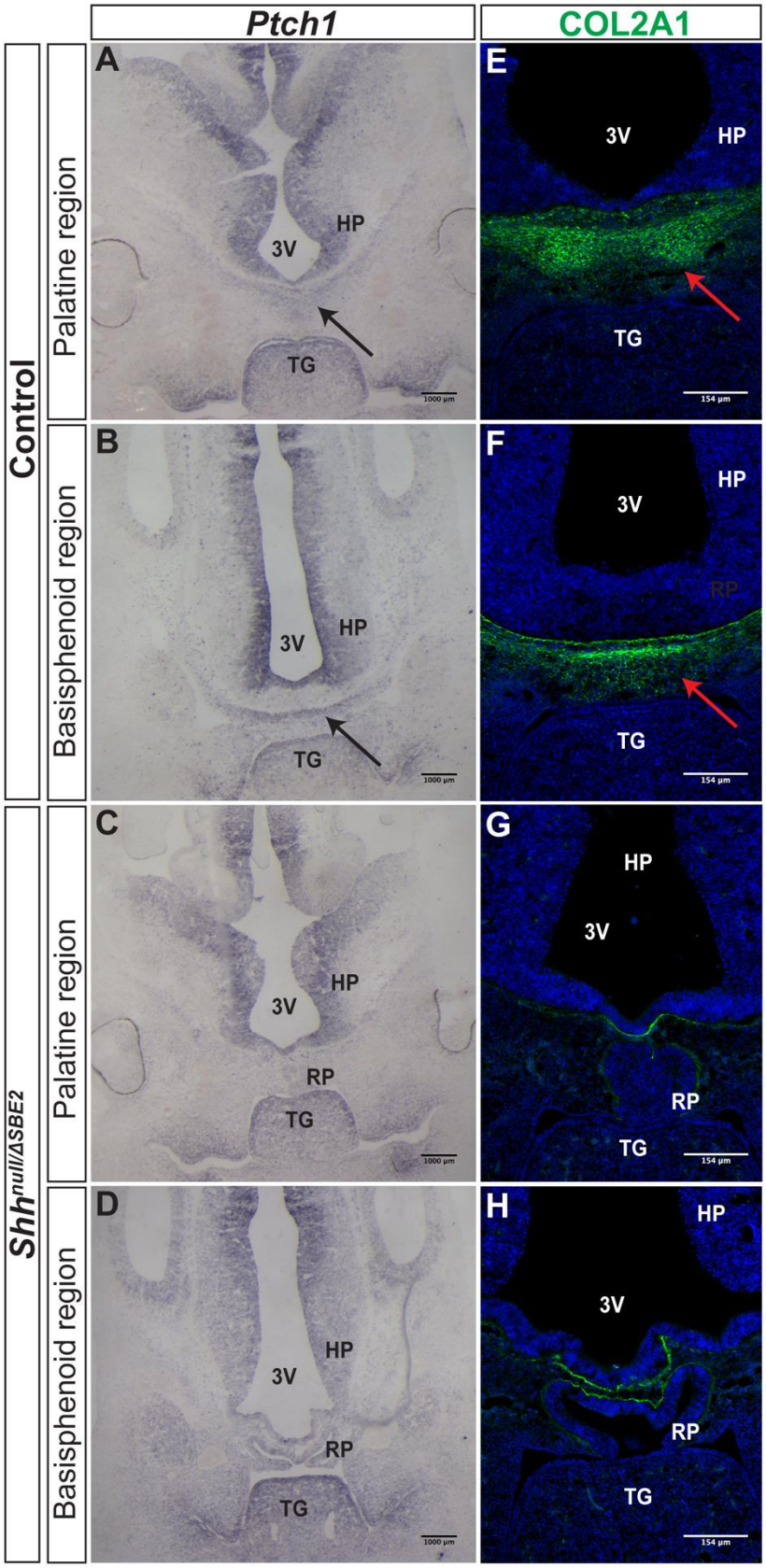
Ptch1
COL2A1
Control
Shh null/ΔSBE2
Palatine region
Basisphenoid region
Palatine region
Basisphenoid region
A
B
C
D
E
F
G
H
3V
HP
TG
RP
1000 µm
154 µm

Figure 4.

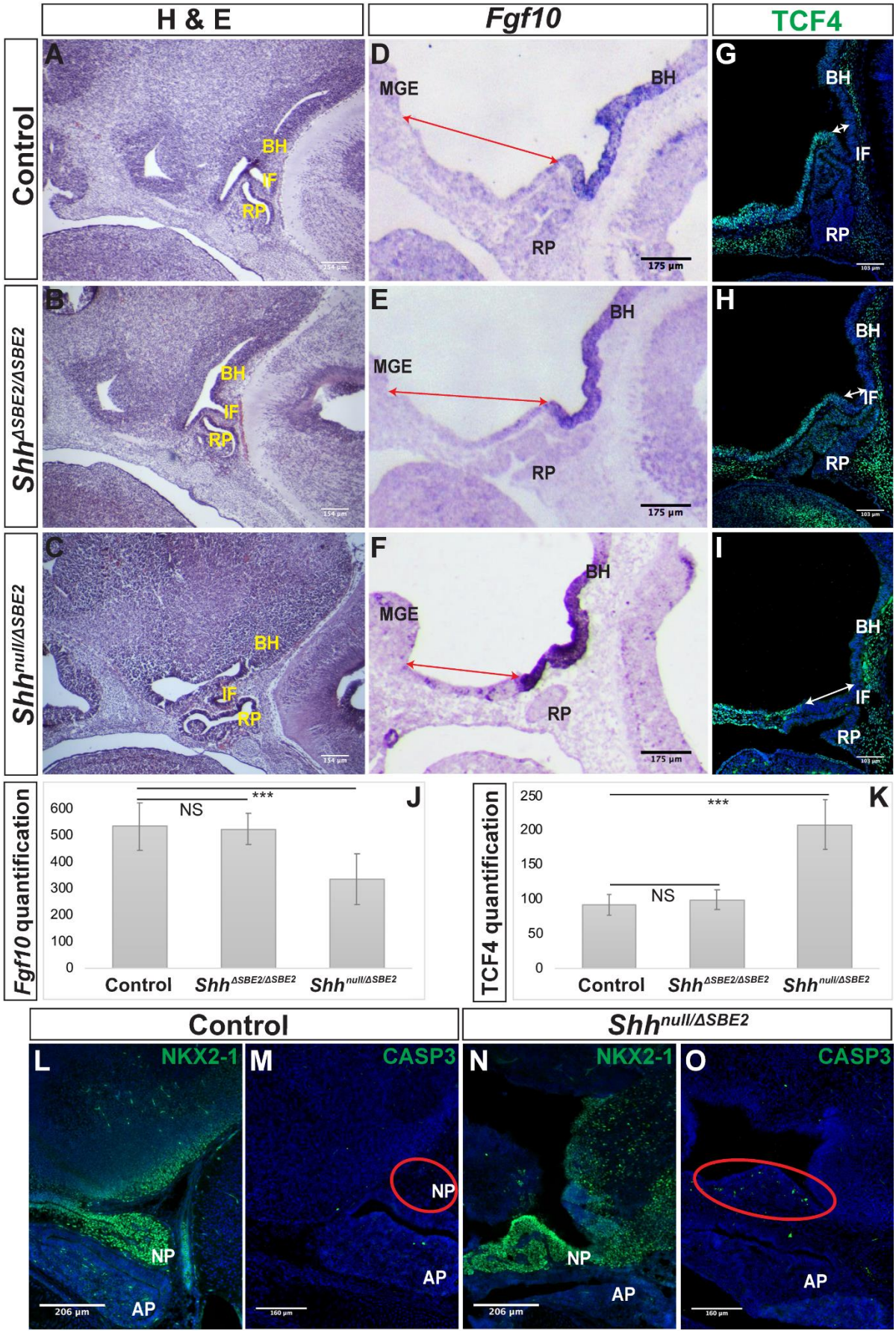
H & E
Fgf10
TCF4
Control
Shh ΔSBE2/ΔSBE2
Shh null/ΔSBE2
A
B
C
D
E
F
G
H
I
BH
IF
RP
MGE
175 µm
Fgf10 quantification
TCF4 quantification
J
K
NS
***
Control
Shh ΔSBE2/ΔSBE2
Shh null/ΔSBE2
L
M
N
O
NKX2-1
CASP3
NP
AP
206 µm
160 µm

Figure 5.

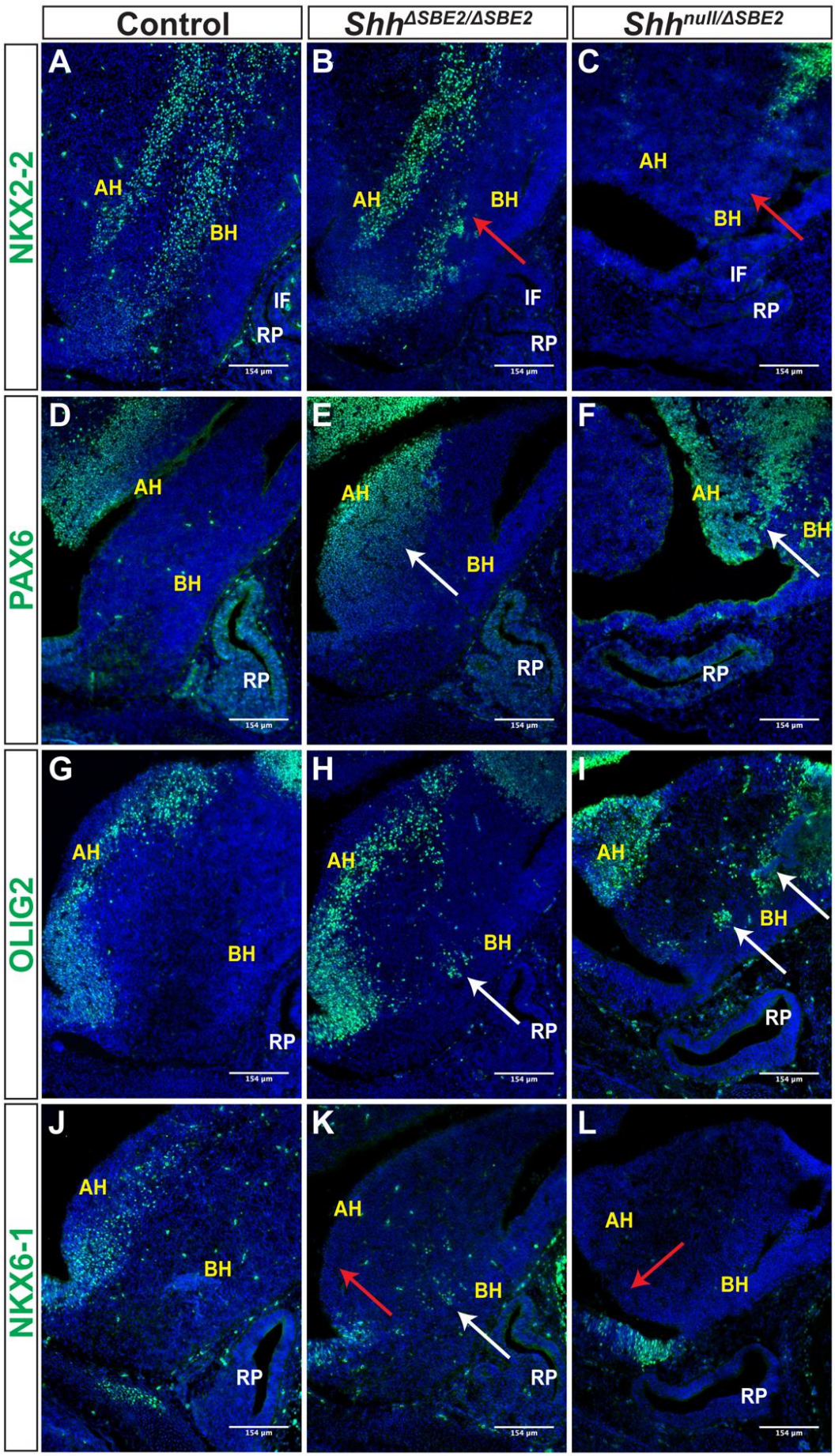
Control
Shh ΔSBE2/ΔSBE2
Shh null/ΔSBE2
NKX2-2
PAX6
OLIG2
NKX6-1
A
B
C
D
E
F
G
H
I
J
K
L
AH
BH
IF
RP
154 µm

Figure 6

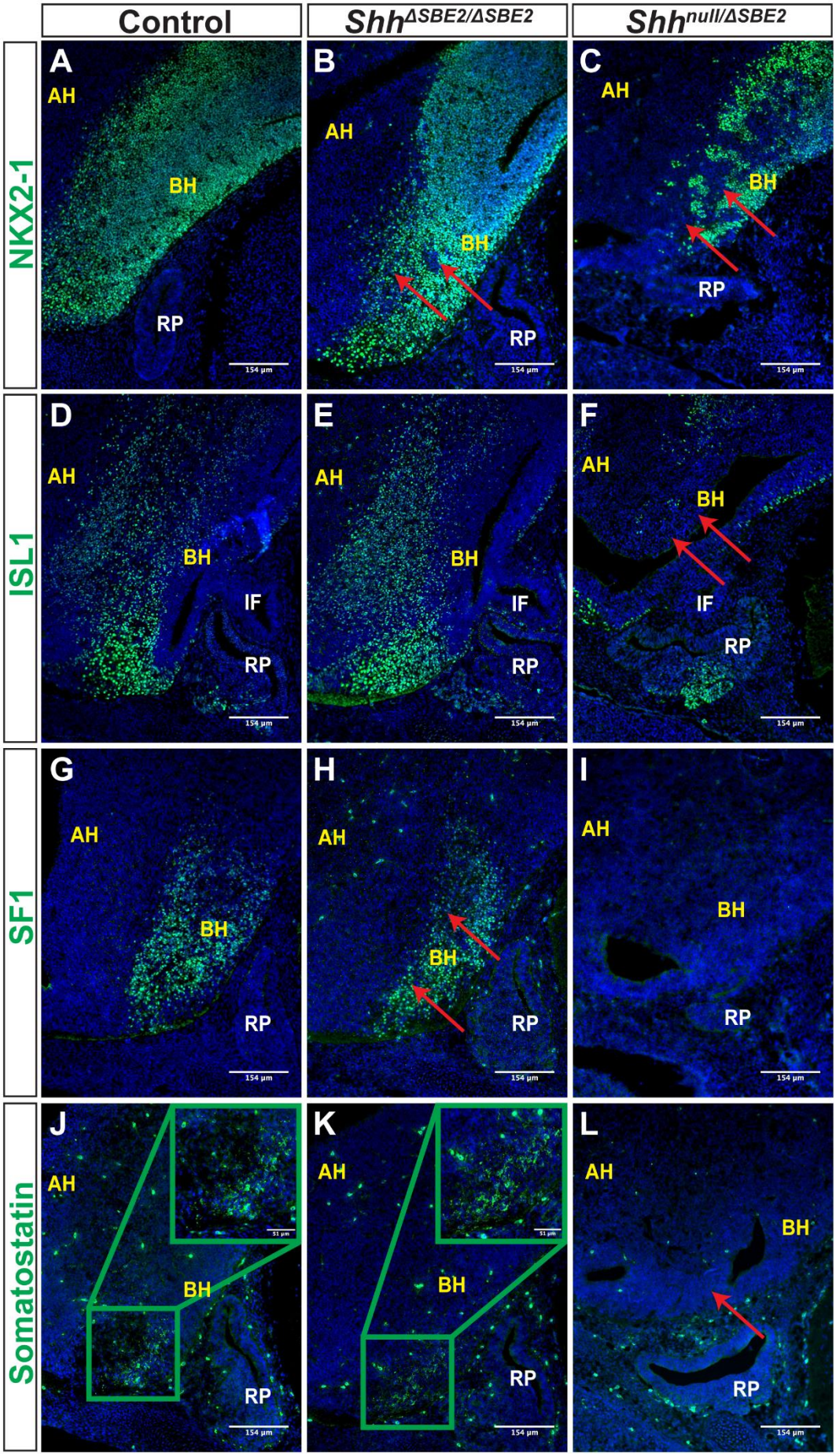
Control
Shh ΔSBE2/ΔSBE2
Shh null/ΔSBE2
NKX2-1
ISL1
SF1
Somatostatin
A
B
C
D
E
F
G
H
I
J
K
L
AH
BH
RP
IF
154 µm
51 µm

Figure 7